

Bardeen-de Sitter black holes

Sharmanthie Fernando ¹

Department of Physics, Geology & Engineering Technology

Northern Kentucky University

Highland Heights

Kentucky 41099

U.S.A.

Abstract

In this paper we present a regular black hole with a positive cosmological constant. The regular black hole considered is the well known Bardeen black hole and it is a solution to the Einstein equations coupled to non-linear electrodynamics with a magnetic monopole. The paper discuss the properties of the Bardeen-de Sitter black hole. We have computed the grey body factors and partial absorption cross sections for massless scalar field impinges on this black hole with the third order WKB approximation. A detailed discussion on how the behavior of the grey body factors depend on the parameters of the theory such as the mass, charge and the cosmological constant is given. Possible extensions of the work is discussed at the end of the paper.

Key words: static, magnetic charge, regular, Bardeen, black holes, absorption cross sections, de Sitter

1 Introduction

There are many observations that have verified that the present day universe is undergoing accelerated expansion [1][2][3][4]. The common wisdom is that there is some unknown “dark energy” that is causing this accelerated expansion. There are various models that have been proposed in order to explain dark energy, but the cosmological constant seems to be the most popular of all. When a positive cosmological constant is introduced to general theory of relativity, the resulting space time geometry gain a positive curvature asymptotically. Here in this paper we study the Bardeen black hole with a positive cosmological constant. Hence we name this black hole as Bardeen-de Sitter black hole. This is one of few regular black holes with a non-flat asymptotic geometry.

¹fernando@nku.edu

Usually, a black hole has a horizon as well as a singularity inside the horizon where the curvature scalar goes to infinity. However, there are some black holes which do not have a singularity at the origin. Such black holes are called “regular” black holes. Bardeen in 1968 obtained a black holes solution without a singularity and is now well known as the Bardeen black hole [5]. Bardeen black hole spacetime satisfy the weak energy condition but does not satisfy the strong energy condition. The Einstein’s tensor for the Bardeen black hole is non-zero. 30 years later since Bardeen presented his solution, Ayón-Beato and García proved that the Bardeen black hole can be interpreted as a gravitationally collapsed magnetic monopole arising in a specific form of non-linear electrodynamics [6]. The corresponding Lagrangian for the suggested non-linear electrodynamics was presented. Hence the stress energy tensor of the non-linear electrodynamics given worked as the source for the Einstein’s field equations. Bardeen black hole has attracted lot of attention in the recent past. Stability properties of the Bardeen black hole and other regular black holes were studied by Moreno and Sarbach [7]. Quasinormal modes of Bardeen black holes have been studied by several authors [8] [9] [10]. Profiled spectral lines generated by Keplerian discs orbiting around Bardeen black holes were addressed in [11]. Thermodynamic quantities of the Bardeen black holes were studied by Man and Cheng [12]. The geodesic structure of test particle in Bardeen space-time was studied by Zhou et.al. [13].

A black hole does not act like a perfect black body when waves impinged on it. Instead, a part of the wave will scatter back to infinity due to the gravitational potential of the black hole. Therefore, one can define reflection coefficient (R) and transmission coefficient (T) which depends on the frequency of the wave. The grey body factor, $\gamma_l(\omega)$ can be defined as the probability of the waves impinges on the black hole to be absorbed by the black hole. In terms of the transmission coefficient, the grey body factor, $\gamma_l(\omega) = |T|^2$.

Studying the absorption and scattering cross sections of waves by black holes has been done since 1970’s. There are many works dedicated to calculate greybody factors, absorption cross sections in the literature. It is not possible to include all of the works related to grey body factors, but will mention some of the interesting works we found in the literature. Greybody factors for scalar fields emitted by higher-dimensional Schwarzschild-de Sitter black holes were studied by Kanti et.al. [14]. The temperature dependence of the absorption cross section for black holes in string theory is given in [15]. Greybody factors for topologically massless black holes for non-minimally coupled scalar field is studied by Gonzalez et.al[16]. In [17], absorption cross section in de Sitter space in three dimensions were studied. Massless scalar field emission in 2+1 dimensional dilaton charged black holes were studied by Fernando [18]. Black hole grey body factors and D-brane spectroscopy were studied by Maldesena and Strominger [19]. Since we are studying the Bardeen black hole in this paper, we would like to mention works that have addressed absorption cross sections of such black holes: absorption cross section for the Bardeen black hole with $\Lambda = 0$ was done in [20], [21] [22] and [23].

2 Introduction to the Bardeen-de Sitter black hole

In this section, we will extend the work of [6] to include a cosmological constant to the theory. The corresponding action is given by,

$$S = \int d^4x \sqrt{-g} \left[\frac{(R - 2\Lambda)}{16\pi} - \frac{1}{4\pi} \mathcal{L}(F) \right] \quad (1)$$

Here, R is the scalar curvature, and $\mathcal{L}(F)$ is a function of $F = \frac{1}{4} F_{\mu\nu} F^{\mu\nu}$ given by,

$$\mathcal{L}(F) = \frac{3}{2sg^2} \left(\frac{\sqrt{2g^2 F}}{1 + \sqrt{2g^2 F}} \right)^{\frac{5}{2}} \quad (2)$$

The field strength of the non-linear electrodynamics, $F_{\mu\nu}$ is given by,

$$F_{\mu\nu} = 2(\nabla_\mu A_\nu - \nabla_\nu A_\mu) \quad (3)$$

The parameter s in the above equation is given by $s = \frac{|g|}{2M}$ where g and M corresponds to the magnetic charge and the mass of the black hole.

The field equations of motion derived from the action in eq(1) is given by,

$$G_{\mu\nu} + \Lambda g_{\mu\nu} = 2 \left(\frac{\partial \mathcal{L}(\mathcal{F})}{\partial F} F_{\mu\lambda} F_\nu^\lambda - g_{\mu\nu} \mathcal{L}(\mathcal{F}) \right) \quad (4)$$

$$\nabla_\mu \left(\frac{\partial \mathcal{L}(\mathcal{F})}{\partial F} F^{\nu\mu} \right) = 0 \quad (5)$$

$$\nabla_\mu (*F^{\nu\mu}) = 0 \quad (6)$$

We will look for space-time solutions which are static and spherically symmetric for the above set of equations with a metric as follows:

$$ds^2 = -f(r)dt^2 + f(r)^{-1}dr^2 + r^2(d\theta^2 + \sin^2(\theta)d\varphi^2) \quad (7)$$

where,

$$f(r) = 1 - \frac{2m(r)}{r} \quad (8)$$

For a spherically symmetric space-time, the only non-vanishing components for $F_{\mu\nu}$ are F_{01} and F_{23} . We will follow the same ansatz made in [6] for the Maxwell field as,

$$F_{\mu\nu} = 2\delta_{[\mu}^\theta \delta_{\nu]}^\varphi Z(r, \theta) \quad (9)$$

When this ansatz is substituted to eq.(5), it can be integrated easily to obtain,

$$F_{\mu\nu} = 2\delta_{[\mu}^\theta \delta_{\nu]}^\varphi g(r) \sin\theta \quad (10)$$

The eq.(6), implies $dF = 0$; Hence $g'(r)\sin\theta dr \wedge d\theta \wedge d\varphi = 0$, which lead to the conclusion that $g(r) = \text{const} = g$. Here g is the magnetic monopole charge. Hence, the magnetic field strength is given by,

$$F_{23} = 2g\sin\theta \quad (11)$$

and

$$F = \frac{g^2}{2r^4} \quad (12)$$

By substituting the value of F in eq.(12) to eq.(2) one can obtain,

$$\mathcal{L}(\mathcal{F}) = \frac{3Mg^2}{(r^2 + g^2)^{\frac{5}{2}}} \quad (13)$$

From the Einstein field equations, eq(4), the G_{tt} component can be written as,

$$G_{tt} + \Lambda g_{tt} = -2\mathcal{L}(\mathcal{F})g_{tt} \quad (14)$$

where,

$$G_{tt} = -2 \left(1 - \frac{2m(r)}{r} \right) \frac{m'(r)}{r^2} \quad (15)$$

By substituting eq(15) and eq(13) into eq(14), one get,

$$m'(r) - \frac{\Lambda r^2}{2} = \frac{3Mg^2 r^2}{(r^2 + g^2)^{\frac{5}{2}}} \quad (16)$$

Integrating eq(16) from r to ∞ , one get,

$$-m(r) + \frac{\Lambda r^3}{6} + \text{constant} = \int_r^\infty \frac{3Mg^2 r^2}{(r^2 + g^2)^{\frac{5}{2}}} \quad (17)$$

Here,

$$\text{constant} = \lim_{r \rightarrow \infty} \left(m(r) - \frac{\Lambda r^3}{6} \right) = M \quad (18)$$

The last integral in eq(17) leads to an exact result given by,

$$\int_r^\infty \frac{3Mg^2 r^2}{(r^2 + g^2)^{\frac{5}{2}}} = M - \frac{Mr^3}{(g^2 + r^2)^{\frac{3}{2}}} \quad (19)$$

Finally, the function $m(r)$ is given by,

$$m(r) = \frac{\Lambda r^3}{6} + \frac{Mr^3}{(g^2 + r^2)^{\frac{3}{2}}} \quad (20)$$

Substituting the expression for $m(r)$ in to the $f(r)$, one get,

$$f(r) = 1 - \frac{2Mr^2}{(r^2 + g^2)^{\frac{3}{2}}} - \frac{\Lambda r^2}{3} \quad (21)$$

2.1 Horizons of the black holes

To determine the horizon structures, one can study the roots of $f(r) = 0$. $f(r) = 0$ leads to the polynomial,

$$r^{10}\Lambda^2 + r^8(3g^2\Lambda^2 - 6\Lambda) + r^6(3\Lambda^2g^4 - 18g^2\Lambda + 9) + r^4(g^6\Lambda^2 - 18g^4\Lambda - 36M^2 + 27g^2) + r^2(27g^4 - 6g^6\Lambda) + 9g^6 = 0 \quad (22)$$

There can be three real roots, one real root or degenerate roots for the above equation. Fig(1) demonstrates different root structure for $f(r)$. The Bardeen-de Sitter black hole could have three horizons: inner horizon(r_i), event horizon(r_h) and the cosmological horizon(r_c). It can have degenerate horizons when two of these merge. It can also have only one horizon (cosmological horizon) for certain values of the parameters of the theory. We have also plotted the function $f(r)$ for the Reissner-Nordstrom-de Sitter black hole and the Bardeen black hole in the same figure which is given in Fig(2). The inner horizon is smaller for the Reissner-Nordstrom-de Sitter black hole compared to the Bardeen-de Sitter black hole. The event horizon is larger for the Reissner-Nordstrom-de Sitter black hole compared to the Bardeen-de Sitter black hole.

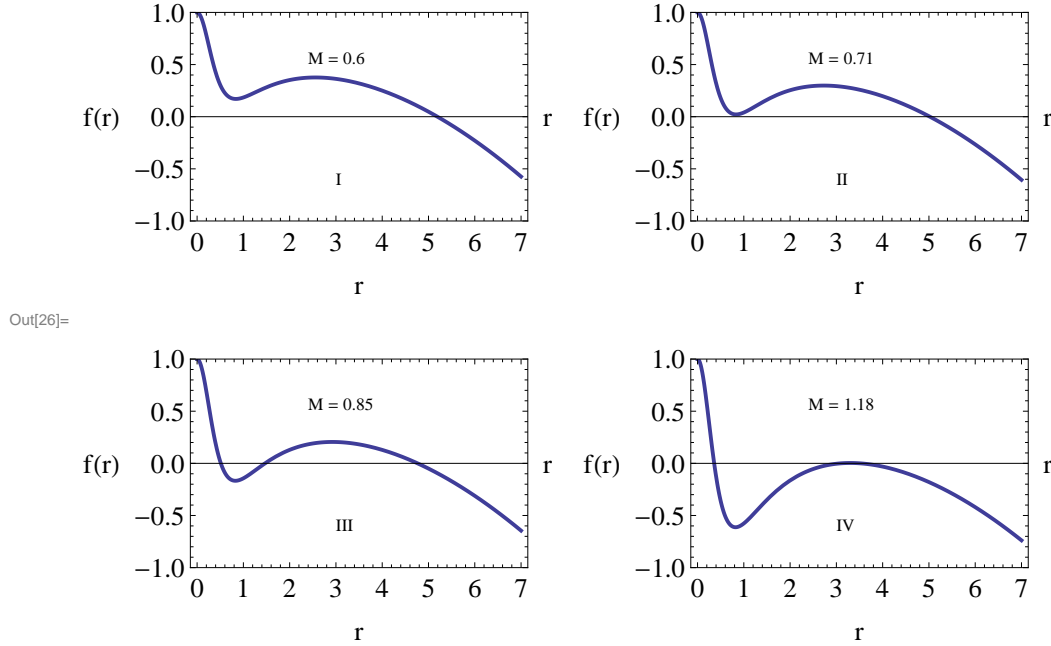


Figure 1: Figure shows $f(r)$ vs r for $\Lambda = 0.086$ and $g = 0.57$. The mass M is varied to obtain different horizon structures.

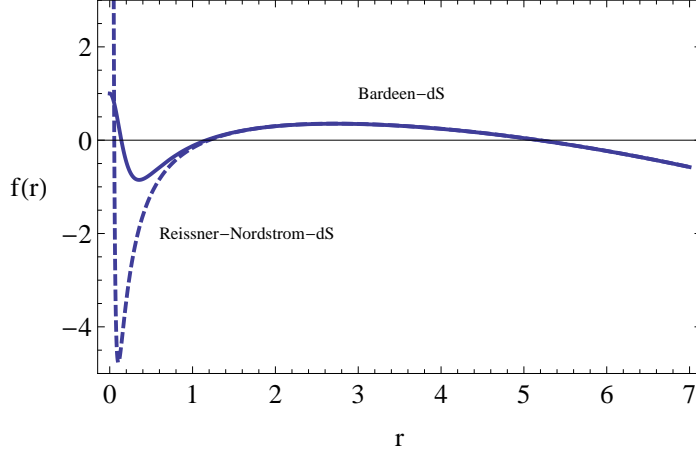


Figure 2: Figure shows $f(r)$ vs r for Reissner-Nordstrom-de Sitter and Bardeen-de Sitter black holes. Here $\Lambda = 0.086$, $M = 0.6$ and $g = 0.25$

The Bardeen-de Sitter black hole is non-singular everywhere since all the scalar curvatures, R , $R_{\mu\nu}R^{\mu\nu}$ and $R_{\mu\nu\alpha\beta}R^{\mu\nu\alpha\beta}$ are finite everywhere. Only the electromagnetic invariant $F = \frac{g^2}{2r^4}$ has singular behavior at $r = 0$. The Bardeen-de Sitter black hole satisfy the weak energy condition.

Asymptotically, the metric function $f(r)$ behaves as,

$$f(r) \approx 1 - \frac{2M}{r} + \frac{3Mg^2}{r^3} - \frac{\Lambda r^2}{3} + O\left(\frac{1}{r^5}\right) \quad (23)$$

2.2 Extreme black holes

Bardeen-de Sitter black hole could have degenerate horizons depending on the parameters M, g and Λ . Degenerate horizons occur when $f(r) = f'(r) = 0$. We will discuss three different types of degenerate black holes that may occur.

2.2.1 Nariai black holes

When the cosmological and the event horizon merge, one get Nariai black holes. This special case is represented by the Figure.(1) (IV). In these black holes, the degenerate horizon is given by,

$$r_{Na}^2 = \frac{1 + \sqrt{1 - 8g^2\Lambda}}{2\Lambda} \quad (24)$$

The corresponding mass is given by,

$$M_{Nariai} = \frac{(g^2 + r_{Na}^2)^{5/2}\Lambda}{3(r_{Na}^2 - 2g^2)} \quad (25)$$

In obtaining eq.(25), we have substituted r_{Na} to $f'(r_{Na}) = 0$.

From eq(24), one can see that the degenerate black holes exists only if $8\Lambda g^2 < 1$.

For a nearly extreme black hole, such as Nariai black hole, one can approximate the function $f(r)$ as,

$$f(r) = \frac{f''(r_{ex})}{2}(r - r_c)(r - r_h) \quad (26)$$

Now, we shall introduce new coordinates, χ and ψ as,

$$r = r_{ex} + \epsilon \cos \chi \quad (27)$$

$$t = \frac{2\psi}{\epsilon f''(r_{ex})} \quad (28)$$

Here ϵ is small. Hence, $\chi = 0$ corresponds to $r = r_{ex} + \epsilon = r_c$ and $\chi = \pi$ corresponds to $r = r_{ex} - \epsilon = r_h$. The new coordinate ψ is time like. One can note that $f''(r_{ex}) < 0$ for the Nariai black hole due to the nature of the function $f(r)$ at $r = r_{ex}$. Now, after substituting the new coordinates, and taking the limit $\epsilon \rightarrow 0$, the metric simplifies to

$$ds^2 = \frac{2}{f''(r_{ex})} \left(\sin^2 \chi d\psi^2 - d\chi^2 \right) + r_{ex}^2 d\Omega^2 \quad (29)$$

The above geometry corresponds to $dS_2 \times S^2$. The dS_2 has a positive scalar curvature,

$$R_{dS_2} = -f''(r_{ex}) \quad (30)$$

For the Bardeen-de Sitter black hole,

$$f''(r_{ex}) = \frac{2r_{ex}^2 \Lambda (r_{ex}^2 - 4g^2)}{(2g^4 + g^2 r_{ex}^2 - r_{ex}^4)} \quad (31)$$

2.2.2 Cold black holes

When the inner and the outer horizons coincides, one get cold black hole with zero temperature. This special case is represented by Figure 1 (II). Similar to the Nariai black holes, at the degenerate horizons $f(r_{ex}) = f'(r_{ex}) = 0$. Due to the nature of the function $f(r)$ at the horizons, $f''(r_{ex}) > 0$. The horizon of cold black holes are given by,

$$r_{cold}^2 = \frac{1 - \sqrt{1 - 8g^2 \Lambda}}{2\Lambda} \quad (32)$$

The corresponding mass is given by,

$$M_{cold} = \frac{(g^2 + r_{cold}^2)^{5/2} \Lambda}{3(r_{cold}^2 - 2g^2)} \quad (33)$$

Two new coordinates ψ and χ can be introduced as,

$$r = r_{ex} + \epsilon \cosh \chi \quad (34)$$

$$t = \frac{2\psi}{\epsilon f''(r_{ex})} \quad (35)$$

Once again ϵ is small and ψ is a time-like coordinate. Once the new coordinates are substituted to the metric and taken the limit $\epsilon \rightarrow 0$, the metric becomes,

$$ds^2 = -\frac{2}{f''(r_{ex})} \left(\sinh^2 \chi d\psi^2 - d\chi^2 \right) + r_{ex}^2 d\Omega^2 \quad (36)$$

The above geometry represents $AdS_2 \times S^2$. The AdS_2 has the scalar curvature $R_{cold} = -f''(r_{cold})$.

2.2.3 Ultracold black holes

In ultracold black holes, all three horizons coincides leading to the radius of the horizon,

$$r_{ucold} = \frac{1}{\sqrt{2\Lambda}} = 2g \quad (37)$$

Here, $f = f' = f'' = 0$. The mass of the ultracold black hole is given by,

$$M_{ultracold} = \frac{25}{96} \sqrt{\frac{5}{2\Lambda}} \quad (38)$$

To understand the geometry of the ultracold black hole near the degenerate horizon, let us take the metric of the cold black hole in eq(36) and make an additional coordinate transformation as,

$$\chi = \eta \sqrt{\frac{f''(r_{ex})}{2}} = \eta a \quad (39)$$

Here we have taken $a = \sqrt{\frac{f''(r_{ex})}{2}}$. When we substituted this to the metric of the cold-black hole in eq(36), one get,

$$ds^2 = \left(\frac{\sinh(\eta a)}{\eta a} \right)^2 d\psi^2 - d\chi^2 + r_{ex}^2 d\Omega^2 \quad (40)$$

Since $f''(r_{ex}) \rightarrow 0$ for ultracold black holes, one can take the limit $f''(r_{ex}) \rightarrow 0$ of eq(40). Since $\frac{\sinh(\eta a)}{\eta a} \rightarrow 1$, the above metric simplifies to,

$$ds^2 = -\eta^2 d\psi^2 + d\eta^2 + r_{ucold}^2 d\Omega^2 \quad (41)$$

The geometry given by the above metric has the topology, $R^2 \times S^2$. This is similar to the topology of the ultra-cold Reissner-Nordstrom- de Sitter black hole.

Nariai, cold and ultracold black holes of Born-Infeld-de Sitter and quintessence black holes were studied by Fernando in [24][25][26]. Degenerate horizons of regular black holes were studied in [27].

2.3 Thermodynamics

The Hawking temperature of the Bardeen-de Sitter black hole is given by,

$$T = -\frac{1}{4\pi} \left. \frac{dg_{tt}}{dr} \right|_{r=r_h} = \frac{1}{4\pi} \left[\frac{2Mr_h(r_h^2 - 2g^2)}{(g^2 + r_h^2)^{5/2}} - \frac{2\Lambda r_h}{3} \right] \quad (42)$$

Here, r_h is the event horizon of the black hole which is a solution of $f(r) = 0$.

3 Massless scalar perturbation of Bardeen-de Sitter black holes

In this section, we will introduce scalar perturbation by a massless field around the Bardeen black hole. A massless scalar field minimally coupled to gravity is described by the Klein-Gordon equation given by,

$$\frac{1}{\sqrt{-g}} \partial_\mu (\sqrt{-g} \partial^\mu \Phi) = 0 \quad (43)$$

For a monochromatic wave with frequency ω in a spherically symmetric space-time, one can introduce the ansatz for Φ as,

$$\Phi = \sum e^{-i\omega t} Y_{l,m}(\theta, \phi) \frac{\xi(r)}{r} \quad (44)$$

With the ansatz given in eq(44), eq(43) simplifies to a Schrödinger-type equation given by,

$$\frac{d^2 \xi(r)}{dr_*^2} + (\omega^2 - V_s(r_*)) \xi(r) = 0 \quad (45)$$

Here $V_s(r_*)$ is the scalar field potential given by,

$$V_s(r) = \frac{l(l+1)f(r)}{r^2} + \frac{f(r)f'(r)}{r} \quad (46)$$

and r_* is the well known ‘‘tortoise’’ coordinate given by,

$$dr_* = \frac{dr}{f(r)} \quad (47)$$

When $r \rightarrow r_c$, $r_* \rightarrow \infty$ and when $r \rightarrow r_h$, $r_* \rightarrow -\infty$. The potential $V_s(r)$ goes to zero at $r = r_c, r_h$.

From Fig(3), when l is increased, the height of the potential increases. This is the well-known suppression of the emission of modes with large l . Notice that when $l = 0$, there is local minimum between the two horizons for the potential.

When the magnetic charge g is increased, the potential height becomes larger as given in Fig(4) and there will be suppression of scalar field emission. On the other hand, when Λ is increased, the height of the potential decreases as shown in Fig(5) leading to an enhancement of emission of scalar fields.

We also plotted the potentials for the Bardeen-dS and the Schwarzschild-dS black holes in the same graph to compare in Fig(6). It is clear that the Bardeen-dS black hole has a higher potential. Hence the scalar fields are suppressed for the Bardeen-de Sitter black holes as compared with the Schwarzschild-de Sitter black holes.

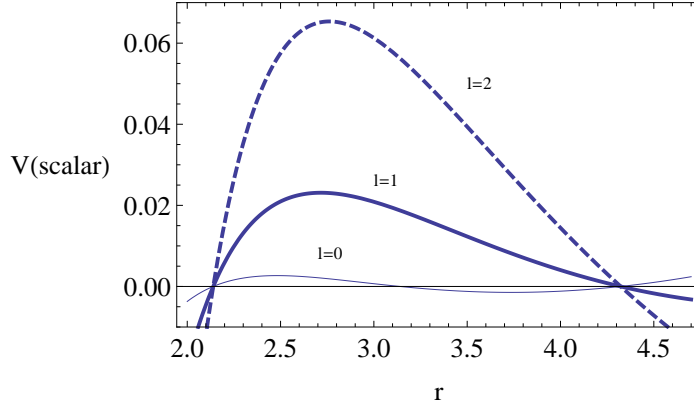


Figure 3: The figure shows $V_s(r)$ vs r for $\Lambda = 0.086, M = 1.03$ and $g = 0.57$

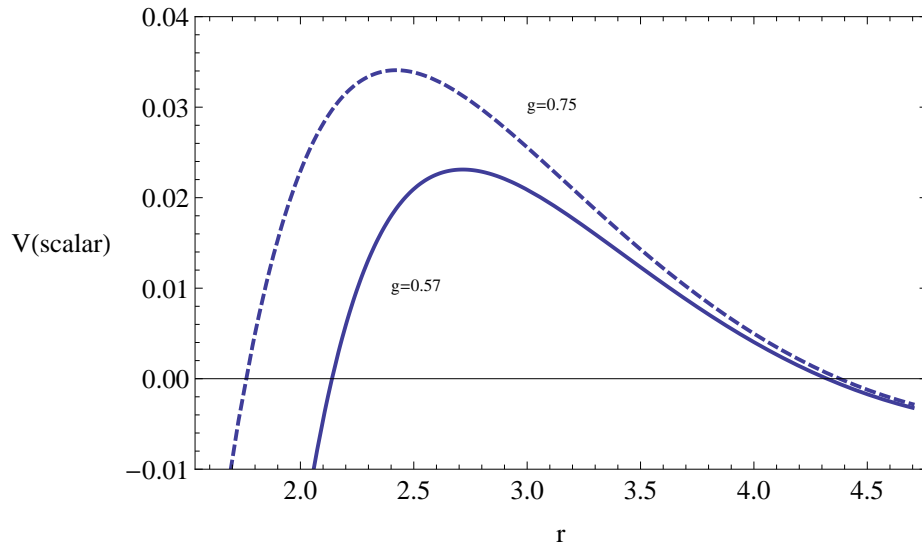


Figure 4: The figure shows $V_s(r)$ vs r for $\Lambda = 0.086, M = 1.03$ and $l = 1$

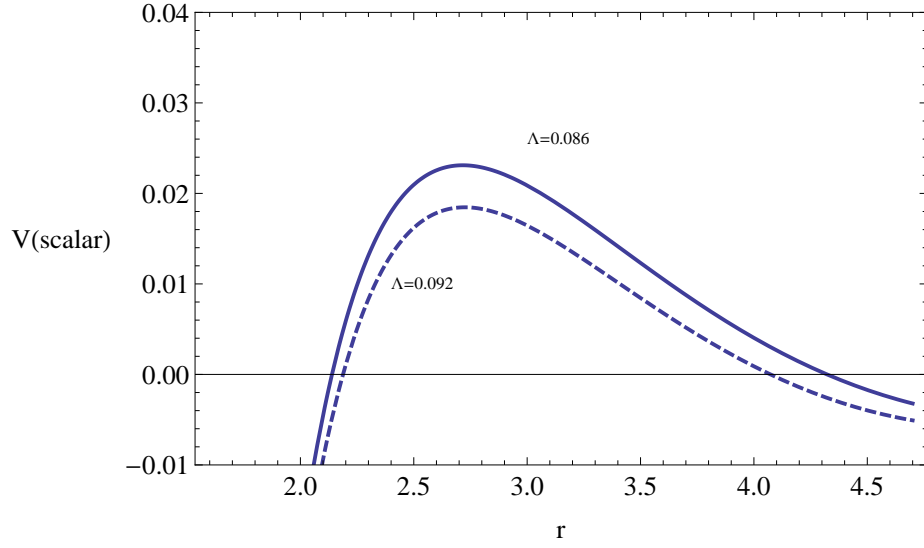


Figure 5: The figure shows $V_s(r)$ vs r for $l = 1$, $M = 1.03$ and $g = 0.57$

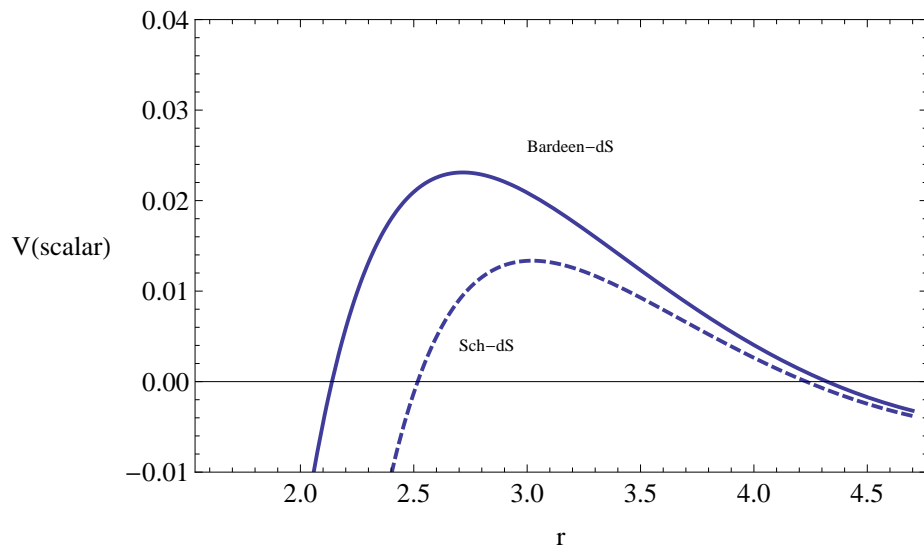


Figure 6: The figure shows $V_s(r)$ vs r for the Bardeen-de Sitter and Schwarzschild-de Sitter black holes. Here, $\Lambda = 0.086$, $M = 1.03$, $l = 1$ and $g = 0.57$

4 WKB approximation method to compute the greybody factors and partial absorption cross sections

In this section we will describe the computation of reflection coefficients, transmission coefficients (greybody factors) and partial absorption cross sections via the WKB approximation. Let us assume a wave is coming from the past cosmological horizon which corresponds to $r_* \rightarrow \infty$ ($r \rightarrow r_c$). When the wave reaches the black hole some of it will be reflected due to the gravitational potential and some of them will be transmitted. The reflected and the transmitted waves can be represented as the following:

$$\xi(r_*) = T(\omega)e^{-i\omega r_*} \quad r_* \rightarrow -\infty (r \rightarrow r_h) \quad (48)$$

$$\xi(r_*) = e^{-i\omega r_*} + R(\omega)e^{i\omega r_*} \quad r_* \rightarrow +\infty (r \rightarrow r_c) \quad (49)$$

Here, $R(\omega)$ and $T(\omega)$ are the reflection and transmission coefficient respectively. They are related by,

$$|R(\omega)|^2 + |T(\omega)|^2 = 1 \quad (50)$$

The greybody factor $\gamma_l(\omega)$ and the partial absorption cross section of the wave for a given frequency ω and l is given by,

$$\gamma_l(\omega) = |T(\omega)|^2 \quad (51)$$

$$\sigma_l = \frac{\pi(2l+1)}{\omega^2} |T(\omega)|^2 \quad (52)$$

4.1 WKB method

In this section, we will describe the calculation of $R(\omega)$ and $T(\omega)$ using the WKB approximation. If r_0 is the value of r where the potential $V_s(r)$ is the maximum, then depending on the relation between ω and $V_s(r_0)$, there are three cases to consider:

(a) $\omega^2 \ll V_s(r_0)$: Here the transmission coefficient is close to zero and the reflection coefficient is almost equal to one.

(b) $\omega^2 \gg V_s(r_0)$: Here the transmission coefficient is close to one and the reflection coefficient is almost equal to zero.

(c) ω^2 is of the same order as $V_s(r_0)$: This is the case where we will focus on. It is known that the WKB approximation has high accuracy when $\omega^2 \approx V_s(r_0)$.

Now, let us describe the WKB method developed by Shutz and Will [28] and Iyer and Will[29]: in this approximation, the reflection coefficient $R(\omega)$ is given by,

$$R(\omega) = \left(1 + e^{-2\pi i\alpha}\right)^{-\frac{1}{2}} \quad (53)$$

and

$$|T(\omega)|^2 = 1 - |R(\omega)|^2 \quad (54)$$

Here,

$$\alpha = \frac{i(\omega^2 - V_s(r_0))}{\sqrt{-2V_s''(r_0)}} - \Gamma_2 - \Gamma_3 \quad (55)$$

In the above equation, $V_s''(r_0)$ is the value of the second derivative of $V_s(r)$ at r_0 . Γ_2 and Γ_3 are the second and third order corrections to the WKB formula beyond the first order approximation. Γ_2 and Γ_3 are given by,

$$\Gamma_2 = \frac{1}{(2Q_0^{(2)})^{1/2}} \left[\frac{1}{8} \left[\frac{Q_0^{(4)}}{Q_0^{(2)}} \right] \left(\frac{1}{4} + \alpha^2 \right) - \frac{1}{288} \left[\frac{Q_0^{(3)}}{Q_0^{(2)}} \right]^2 (7 + 60\alpha^2) \right] \quad (56)$$

$$\begin{aligned} \Gamma_3 = & \frac{n + \frac{1}{2}}{2Q_0^{(2)}} \left[\frac{5}{6912} \left[\frac{Q_0^{(3)}}{Q_0^{(2)}} \right]^4 (77 + 188\alpha^2) - \frac{1}{384} \left[\frac{(Q_0^{(3)})^2 Q_0^{(4)}}{(Q_0^{(2)})^3} \right] (51 + 100\alpha^2) \right. \\ & \left. + \frac{1}{2304} \left[\frac{Q_0^{(4)}}{Q_0^{(2)}} \right]^2 (67 + 68\alpha^2) + \frac{1}{288} \left[\frac{(Q_0^{(2)})^3 Q_0^{(5)}}{(Q_0^{(2)})^2} \right] (19 + 28\alpha^2) - \frac{1}{288} \left[\frac{Q_0^{(6)}}{Q_0^{(2)}} \right] (5 + 4\alpha^2) \right] \end{aligned} \quad (57)$$

Where,

$$Q_0 = \omega^2 - V_s(r) \quad (58)$$

$$Q_0^{(n)} = \left. \frac{d^n Q_0}{dr_*} \right|_{r_* = r_*(r_0)} \quad (59)$$

The WKB method to compute reflection coefficients, transmission coefficients and partial greybody factors have been employed in various papers: greybody factors of black holes in braneworld have been computed by WKB method in [30]. The WKB approach was also used to compute reflection coefficients of zero temperature superconductors by Konoplya and Zhidenko in [31]. Same two authors used 6th order WKB approximation to calculate transmission coefficients of scattering of wormholes [32]

When the cosmological constant is varied, the transmission coefficients (or greybody factors) become larger as given in Fig.(7). This quality is known to be the case for bulk and brane decay of scalar fields for $(4 + n)$ dimensional Schwarzschild-de Sitter black holes [33]. Reflection coefficients correspondingly decreases with Λ as given

in Fig(7). The partial absorption cross section also increases as Λ goes up as given in Fig(8).

When the magnetic charge g is increased, the coefficient of transmission (greybody factors) decreases as in Fig(9). Correspondingly, the reflection coefficient decreases with g . The partial absorption cross section is high for low values of g as given in Fig(10). Hence we notice that the absorption is less for high magnetic charge g values. This is in fact is expected since the height of the effective potential in Fig(4) increases when g is increased. So there is less absorption for large g . Similar behavior was observed for the Bardeen black hole with $\Lambda = 0$ in the paper by Macedo and Crispino in [20].

We have also calculated R , T and σ_l for the Schwarzschild-de Sitter and Bardeen-de Sitter black hole for the same values of Λ , M . As shown in Fig(11), Bardeen-de Sitter has a lower value for T and higher value for R in comparison with the Schwarzschild-de Sitter black hole. The partial absorption cross section is lower for the Bardeen-de Sitter black hole as given in Fig(12). This is in fact in agreement with the effective potentials given in Fig(6) where the height of the Bardeen-de Sitter potential is higher leading to lower absorption.

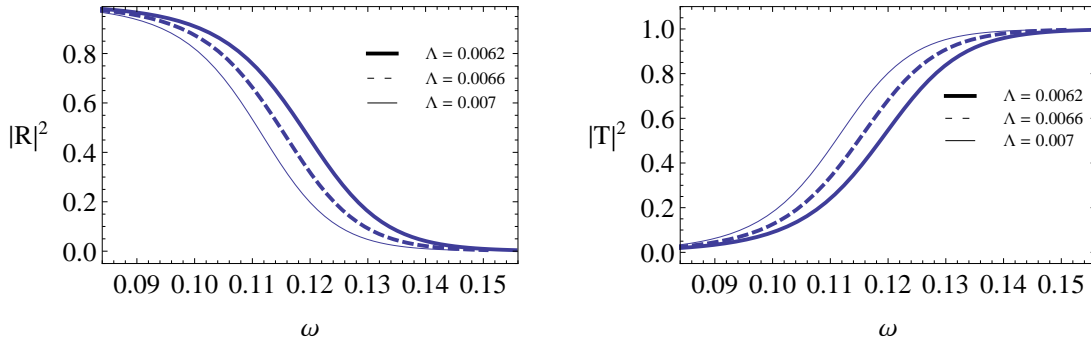


Figure 7: The figure shows $T(\omega)^2$ and $R(\omega)^2$ vs ω for $g = 1$, $M = 3$ and $l = 2$. The value of Λ takes the values 0.0062, 0.0066, 0.007.

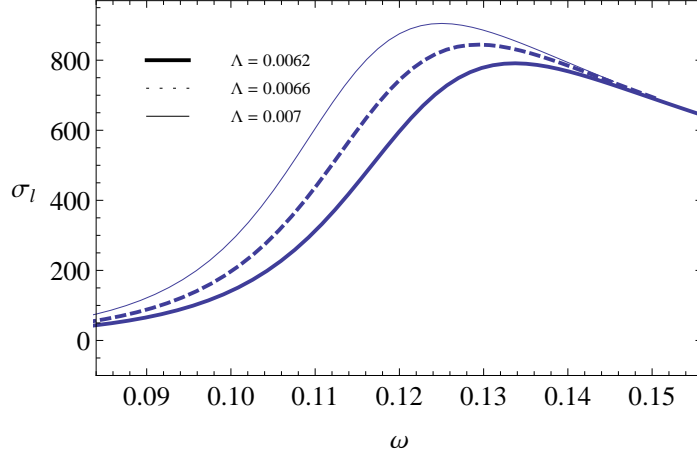


Figure 8: The figure shows $\sigma_l(\omega)$ vs ω for $g = 1, M = 3$ and $l = 2$. The value of Λ takes the values 0.0062, 0.0066, 0.007.

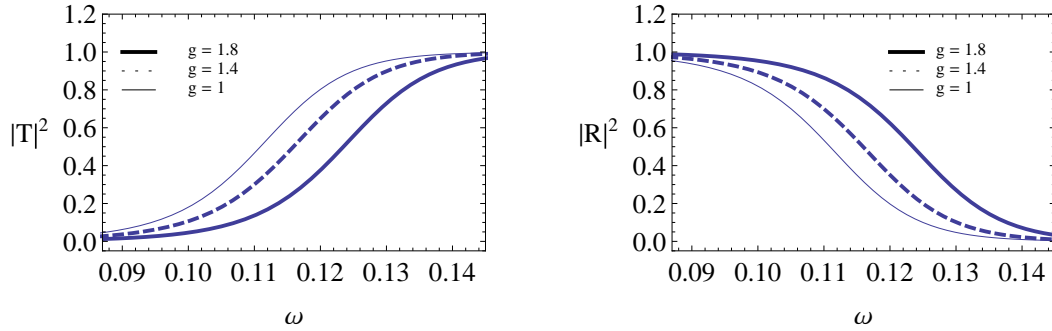


Figure 9: The figure shows $T(\omega)^2$ and $R(\omega)^2$ vs ω for $\Lambda = 0.007, M = 3$ and $l = 2$. The value of g takes the values 1, 1.4, 1.8.

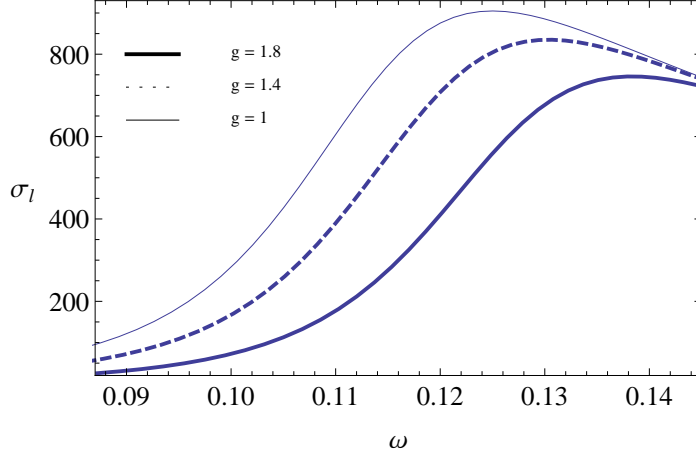


Figure 10: The figure shows $\sigma_l(\omega)^2$ vs ω for $\Lambda = 0.007$, $M = 3$ and $l = 2$. The value of g takes the values 1, 1.4, 1.8.

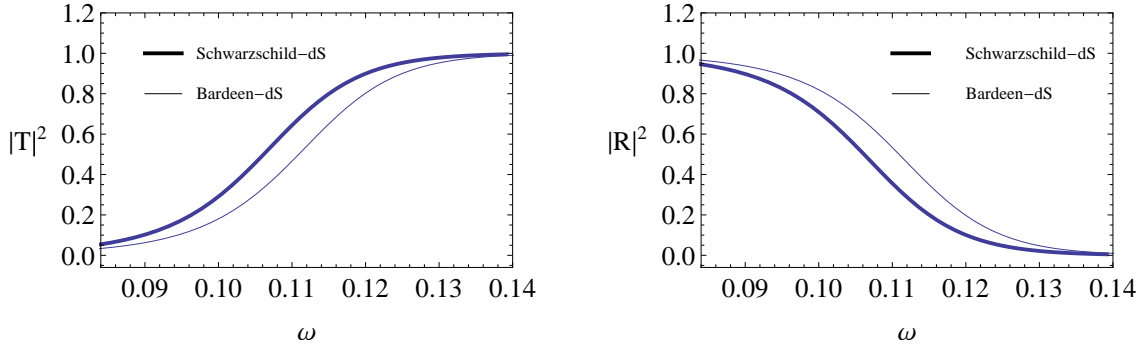


Figure 11: The figure shows $T(\omega)^2$ and $R(\omega)^2$ vs ω for the Schwarzschild-de Sitter and the Bardeen-de Sitter black holes. Here $\Lambda = 0.007$, $M = 3$, $l = 2$ and $g = 1$.

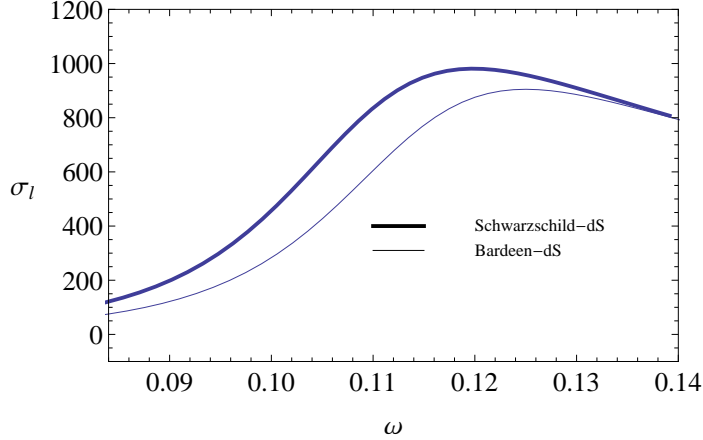


Figure 12: The figure shows σ_l vs ω for the Schwarzschild-de Sitter and the Bardeen-de Sitter black holes. Here $\Lambda = 0.007$, $M = 3$, $l = 2$ and $g = 1$.

5 Discussion

In this paper we have presented a new class of black hole solutions which are regular; it is an extension of the well known Bardeen black hole with a positive cosmological constant. Bardeen dS black hole is regular everywhere as it's counterpart with a $\Lambda = 0$. Such black holes could have three horizons depending on the parameters of the black holes such as M , Λ and the magnetic monopole charge g . We have compared the horizons of the Bardeen dS black hole with the Schwarzschild dS black hole and observed that the event horizon is smaller for the Bardeen dS black hole.

We have discussed the various geometries for the degenerate black holes such as Nariai, cold and ultracold black holes.

The main goal of this paper is to present the scattering information of a massless scalar wave impinged on the Bardeen dS black hole. The effective potentials for the scalar wave is presented for various values of the parameters such as l , g and Λ . When l and g increases, the height of the potentials increase. We also observed that for $l = 0$, the potential has a local minimum between the two horizons which is different compared to other potentials. When Λ is increased, the height of the potential decreases. Schwarzschild dS black hole has a smaller potential than the Bardeen dS black hole.

To calculate the scattering information such as the transmission coefficient (T), reflection coefficient (R) and the partial cross section σ_l , we have employed the third order WKB approach. When the cosmological constant is increased, T (or the grey body factor) and σ_l increases. Hence the presence of Λ enhances the grey body factor and the absorption. When the magnetic charge g is increased, T and σ_l decreases. Hence the presence of the magnetic charge decreases the absorption. Similar results

have been reported for the the Bardeen black hole with $\Lambda = 0$. We also compared the values for σ_l and T for the Schwarzschild dS and the Bardeen dS black hole.

In continuing this work, it would be interesting to do a comparison of grey body factors of Reissner-Nordstrom-de Sitter black hole and the Bardeen de Sitter black hole with the same charge. Also, computation of the quasi normal modes for this black hole for the spin 0, $\frac{1}{2}$ and 2 would be interesting. In this work, we have not computed the $l = 0$ case since the potential has a local minimum and the WKB approach is not effective. Another numerical method, such as the Runge-Kutta method would be appropriate to calculate cross sections for such a case.

Acknowledgements: SF like to thank A. Zhidenko for providing the *Mathematica* file for the WKB approximation.

References

- [1] S. Perlmutter et. al., *Measurements of Ω and Λ from 42 high-redshift supernovae*, *Astrophys. J.* **517** 565 (1999)
- [2] A.G. Riess et. al., *Observational evidence from supernovae for an accelerating universe and a cosmological constant*, *Astron. J.* **116** 1009 (1998); *BVRI Light Curves for 22 Type Ia Supernovae*, *Astron. J.* **117** 707(1999)
- [3] D. N. Spergel et.al. (WMAP Collaboration), *Wilkinson Microwave Anisotropy Probe (WMAP) three year results: implications for cosmology*, *Astrophys. J. Suppl.* **170** 377 (2007)
- [4] U. Seljak et.al., *Cosmological parameter analysis including SDSS Ly α forest and galaxy bias: constraints on the primordial spectrum of fluctuations, neutrino mass, and dark energy*, *Phys. Rev. D* **71** 103515 (2005)
- [5] J. Bardeen, *Proceedings of GR5, Tiflis, U.S.S.R.* page 174 (1968)
- [6] E. Ayón-Beato and A. García, *The Bardeen model as a nonlinear magnetic monopole*, *Phys. Lett B* **493** 149 (2000)
- [7] C. Moreno & O. Sarbach, *Stability properties of black holes in self-gravitating non-linear electrodynamics*, *Phys. Rev. D* **67** 024028 (2003)
- [8] S. Fernando & J. Correa, *Quasi-normal modes of the Bardeen black hole: scalar perturbations*, *Phys. Rev. D* **86** 64039 (2012)
- [9] A. Flachi & J. Lemos, *Quasinormal modes of regular black holes* *Phys. Rev. D* **87** 024034 (2013)

- [10] S. C. Ulhoa, *On Quasinormal Modes for Gravitational Perturbations of Bardeen Black Hole*, Braz. Jour. Phys. **44** 380 (2014)
- [11] J. Schee & Z. Stuchlík, *Profiled spectral lines generalized by Keplerian discs orbiting in the Bardeen and Ayon-Beato-Garcia spacetimes*, arXiv:1604.00632
- [12] J. Man & H. Cheng, *The calculation of thermodynamic quantities of the Bardeen black holes*, Gen. Rel. Grav. **46** 1559 (2014)
- [13] S. Zhou, J. Chen, & Y. Wang, *Geodesics structure of test particle in Bardeen spacetime*, Int. Jour. Mod. Phys. **D 21** 1250077 (2012)
- [14] P. Kanti, T. Pappus, & N. Pappus, *Greybody factors for scalar fields emitted by a higher-dimensional Schwarzschild-de Sitter black holes*, Phys. Rev. **D 90** 124077 (2014)
- [15] F. Moura, *On the temperature dependence of the absorption cross section for the black holes in string theory*, Int. Jour. Mod. Phys. **D 24** 1542011 (2015)
- [16] P. Gonzalez, J. Saavedra, C. Campuzano, & E. Rojas, *Grey body factors for topological massless black holes*, JHEP 1006:103, (2010)
- [17] Y. S. Myung, *Absorption cross section in de Sitter space*, Mod. Phys. Lett. **A 18** 617 (2003)
- [18] S. Fernando, *Greybody factors of charged dilaton black holes in 2+1 dimensions*, Gen. Rel. Grav. **37**, 461 (2005)
- [19] J. Maldesena & A. Strominger, *Black hole greybody factors and D-brane spectroscopy*, Phys. Rev. **D 55** 861 (1997)
- [20] C. F. B. Macedo, L. C. B. Crispino, *Absorption of planar massless scalar waves by Bardeen regular black hole*, Phys. Rev. **D 90** 064001 (2014)
- [21] C. F. B. Macedo, E. S. de Oliveira, & L. C. B. Crispino, *Scattering by regular black holes: Planar massless scalar waves impinging upon a Bardeen black hole*, Phys. Rev. **D 92** 024012 (2015)
- [22] C. F. B. Macedo, L. C. B. Crispino & E. S. de Oliveira, *Scalar waves in regular Bardeen black holes: Scattering, absorption and quasinormal modes* arXiv:1605.00123
- [23] B. Toshmatov, A. Abdujabbarov, Z. Stuchlik, & B. Ahmedov, *Quasinormal modes of test fields around regular black holes*, Phy. Rev. **D 91** 083008 (2015)
- [24] S. Fernando, *Cold, ultracold and Nariai black holes with quintessence*, Gen. Rel. Grav. **45** 2053 (2013)

- [25] S. Fernando, *Nariai black holes with quintessence*, Mod. Phys. Lett. A **28** 13550189 (2013)
- [26] S. Fernando, *Born-Infeld-de Sitter gravity: cold, ultracold and Nariai black holes*, Int. Jour. Mod. Phys. D **22** 1350080 (2013)
- [27] J. Matyjasek, P. Sauriski & D. Tryniecki, *Inside the degenerate horizons of regular black holes*, Phys. Rev. **D 87** 124025 (2013)
- [28] S. Iyer & C.M. Will, *Black-hole normal modes: A WKB approach. I. Foundations and application of a higher-order WKB analysis of potential-barrier scattering*, Phys. Rev. **D 35** 3621(1987)
- [29] B. F. Schutz & C. M. Will, *Black hole normal modes; A semianalytic approach*, Astrophys. Jour. **291** L33 (1985)
- [30] B. Toshmatov, Z. Stuchlik, J. Schee, & B. Ahmedov, *Quasinormal frequencies of black hole in braneworld*, arXiv:1605.02058
- [31] R. A. Konoplya & A. Zhidenko, *Holographic conductivity of zero temperature superconductors*, Phys. Lett. **B 86** 199 (2010)
- [32] R. A. Konoplya & A. Zhidenko, *Passage of radiation through wormholes of arbitrary shape*, Phys. Rev. **D 81** 124036 (2010)
- [33] P. Kanti, J. Grain, & A. Barrau, *Bulk and brane decay of a $(4+n)$ -dimensional Schwarzschild-de Sitter black hole: scalar radiation*, Phys. Rev. **D 71** 104002 (2005)